Trapping and Manipulation of Biological Particles Through a Plasmonic Platform

Xiaoyu Miao, *Student Member, IEEE*, and Lih Y. Lin, *Senior Member, IEEE*

Abstract—Enhanced optical radiation force can be induced through the resonant scattering field from a single plasmonic nanoparticle or a randomly distributed plasmonic nanoparticle array. In this paper, we utilized the dipole approximation for the Mie scattering field to analyze such radiation force in both far-field and near-field regime. This force can be utilized to develop noninvasive probes for trapping and manipulation of single biological particles. The trapping of single yeast cells is also demonstrated as an application of this approach.

Index Terms—Biological particles, Mie scattering, optical trapping, plasmonics.

I. INTRODUCTION

LOCALIZED surface plasmon resonance (LSPR), a unique phenomenon for noble metal nanoparticles, has been studied actively in recent years [1]–[3]. Various applications based on the LSPR have been developed including biodetection [4], [5], controlled modulation of drug delivery [6], noninvasive cancer therapy [7], microfluidic guiding [8] and mixing [9], nanoscale optical waveguiding [10], and lithography [11].

Parallel to these research efforts, unique properties of LSPR suggest new promising breakthroughs in the area of optical trapping and manipulation of micro/nanoscale objects, including various biological particles. Thus far, optical tweezers, which were invented by scientists at AT&T Bell Laboratories in early 1970s, have been the main and powerful tools for such applications [12]. Optical tweezers have been applied to trap and manipulate biological particles including cells, cellular components, molecular motors, viruses, etc. [13] One drawback of optical tweezers has been the required tight focusing and high optical power of the laser beam, which limits the exposure time of trapped specimens. The requirement on optical intensity can be reduced by combining conventional dielectrophoresis with optically induced conductivity change [14].

Thanks to the electric field enhancement due to LSPR effect, the illumination intensity of the excitation light can be significantly reduced for the trapping purpose. Therefore, many undesirable effects such as photodamage [15], [16] and thermotaxis [17], [18] can be avoided while trapping biological particles. The manipulation capability at low optical powers also has important applications in materials science, for example, to avoid molecular realignment when manipulating particles or defects in liquid crystals [19], [20]. Previously, several research groups reported theoretical studies about the plasmon enhanced optical trapping by using the metal tip [21], nanoaperture [22], and apertureless probe [23]. We have studied theoretically and demonstrated experimentally by using LSPR of a randomly distributed Au nanoparticle array for this application [24]. Parallel and selective trapping in a patterned plasmonic-landscape of an ordered Au disk array has also been demonstrated by Quidant *et al*. [25]. These studies and demonstrations show a promising future for optical manipulation and trapping through plasmonics.

In this paper, we conduct in-depth theoretical study on the induced optical radiation force through resonant scattering field of a single Au nanosphere, and a random distributed Au nanosphere array in both near-field and far-field regimes. We start by studying the far-field and near-field scattering efficiency of an Au nanosphere through Mie theory, and show that the dipole approximation can be applied to describe the scattering field of Au nanosphere when the sphere size is small as compared to wavelength. By applying the dipole approximation, the scattering field from a single resonant Au nanosphere is described as a function of dipolar polarizability. Subsequently, the induced optical radiation force through the resonant scattering field is investigated. Furthermore, we study the scattering field from a randomly distributed Au nanosphere array. The results suggest that such an approach will achieve enhanced optical force, especially for nanosized particles, and may lead to potential applications in developing noninvasive probes for single biological particles with low optical intensity requirement. Experimental demonstration of trapping particles with various sizes down to 1 μm and yeast cells are shown at the end of the paper.

II. LOCALIZED SURFACE PLASMON RESONANCE

A. Semiclassical Model

The resonant electromagnetic behavior of noble metal nanoparticles under light excitation can be explained by the collective oscillation of conduction electrons confined in the nanoparticles. For nanoparticles with a size that is small as compared to wavelength, all the electrons confined in the nanoparticle experience the same electric field, and therefore, move in-phase. The displacement of the electron cloud under the effect of an external electric field leads to the creation of surface charges, positive where the electron cloud is absent and negative where it is accumulating. The dipolar charge separation imposes an effective restoring force on the electron cloud that works against the external field. The resonance occurs where the response of

the electrons shows a $\pi/2$ phase lag with respect to the driving field. Thus, a resonantly enhanced electron oscillation builds up inside the particle, which, in the small particle limit, is homogeneous throughout its volume. This leads to enhanced far-field scattering and absorption cross sections, as well as a strongly enhanced near-field in the vicinity of the particle surface. The peak wavelength for resonance is dependent on the shape and size of the nanoparticle, as well as the dielectric properties of the external medium. Mie theory provides rigorous solution to this problem by solving Maxwell's equation for the scattering of electromagnetic waves by nanospheres.

B. Enhanced Scattering Efficiency

In Mie theory, the far-field scattering efficiency, defined as the ratio of the scattered power in far field to the incident power at the cross section of the nanosphere, is given in the form of the infinite series

$$Q_{\text{fscat}} = \frac{2}{(kR)^2} \sum_{n=1}^{\infty} (2n+1)(|a_n|^2 + |b_n|^2) \qquad (1)$$

where k is the wavenumber, R is the radius of the nanosphere, a_n and b_n are Mie scattering coefficients that are functions of k and R. Physically, Q_{fscat} is a measure of the ability of a metal nanosphere to extract power from an incident wave and redirect it as far-field scattered power over all solid angles.

In near-field region, the electromagnetic waves must be distorted compared to the far field in order to satisfy the boundary conditions at the perfect conductor surface. Therefore, the radial components must be included in the near field while the far field only consists of components perpendicular to the radial direction. A near field scattering efficiency is defined similarly, but the electric field intensity at the surface of the sphere is evaluated. This is given by [26]

$$Q_{\text{nscat}} = 2\left\{ |a_n^2| \left[(n+1)\left|h_{n-1}^{(2)}(kR)\right|^2 + n\left|h_{n+1}^{(2)}(kR)\right|^2 \right] \right.$$
$$\left. + (2n+1)b_n^2 h_n^{(2)}(kR)^2 \right\} \qquad (2)$$

where $h_n^{(2)}$ is the Hankel function of the second kind. Fig. 1 plots the wavelength dependencies of the far-field and near-field scattering efficiency for an Au nanosphere in vacuum with the 60nm radius. The resonance peaks of near-field and far-field scattering spectra are very close to each other but not exactly the same. Typically, the near-field scattering efficiency is much higher than that of the far-field one. This is because most of the scattering field is confined in the near-field regime.

III. DIPOLAR POLARIZABILITY

Equations (1) and (2) show that the electrodynamic response of an isolated nanosphere in the external electric field is a coherent ensemble of an ideal dipole, quadrupole, and higher order multipoles with corresponding size-dependent polarizabilities. The effective polarizabilities can be obtained by dividing each term by the corresponding incident wave amplitude. The lowest order term, i.e., the dipolar polarizability of the nanosphere is
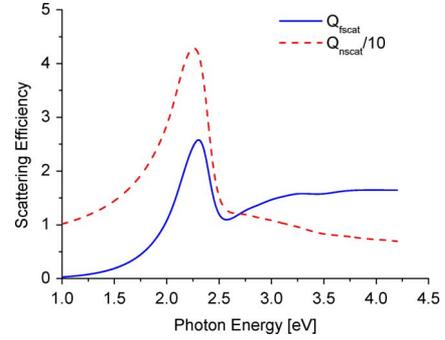

Fig. 1.   Far-field (solid line) and near-field (dash line) scattering efficiencies as a function of photon energy for an Au nanosphere in vacuum with 60 nm radius.
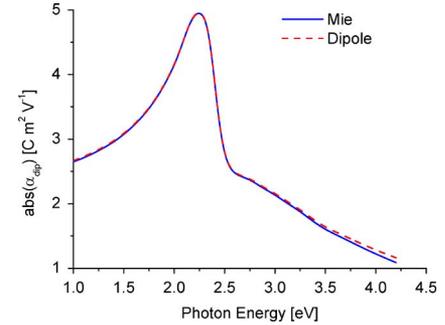

Fig. 2.   Magnitude of the dipolar polarizability of the Au nanosphere in vacuum with the 60 nm radius as a function of photon energy. The solid and dash lines are calculated by (3) (rigorous Mie theory) and (4) (dipole approximation), respectively.

defined as the ratio of the induced dipole moment of the excited nanosphere to the incident electric field. It is given by [27]

$$\alpha_{\text{dip}} = \frac{i6\pi a_1 \varepsilon_0}{k^3} \qquad (3)$$

where a_1 is the first term of the Mie scattering coefficients, ε_0 is the permittivity of free space, and k is the wavenumber in the surrounding medium.

Assuming that the scattering field from the nanosphere is only contributed by the dipolar radiation, the magnitude of the dipolar polarizability of the nanosphere can also be determined from the far-field scattering efficiency, which is given by (Appendix A)

$$|\alpha_{\text{dip}}| = \frac{\sqrt{6Q_{\text{fscat}}}\,\pi R \varepsilon_0}{k^2}. \qquad (4)$$

In Fig. 2, the magnitude of the dipolar polarizability calculated from (4) (dash line in Fig. 2) is slightly larger than the rigorous result obtained from (3) (solid line in Fig. 2), since quadrupole and other higher order components also exist in the scattering field. However, the peak values of the dipolar polarizability calculated through the two different approaches differ by less than 0.097% and both peaks occur at the same wavelength. This suggests that, for such an Au nanosphere at the resonance condition, the dipolar radiation dominates in the scattering field and the multipole components are almost negligible.
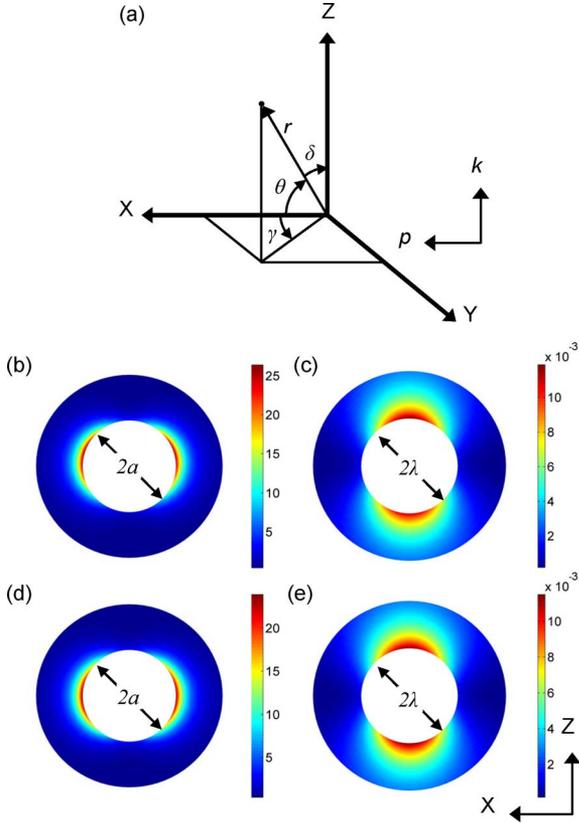
Fig. 3. (a) Geometry definition for calculating the scattering field of a linearly polarized plane wave by an Au nanosphere, where the polarization direction points along the X-axis, the wave vector of the incident wave points along the Z-axis, δ is the intersection angle between the radial vector and the Z-axis, θ is the intersection angle between the radial vector and the X-axis, and γ is the intersection angle between the X-axis and the projection of the radial vector on the XY-plane. (b) Near-field scattering intensity distribution outside a radiating Au nanosphere ($R = 60\,\text{nm}$) in vacuum. The sphere is excited by the plane wave at the resonant wavelength of $540\,\text{nm}$. (c) Far-field scattering intensity distribution outside the nanosphere as in (b). (d) Near-field intensity distribution outside an ideal dipole with the same dipole moment as the Au nanosphere in (a). (e) Far-field intensity distribution outside a dipole as in (d). All the intensity distributions are plotted in the XZ-plane. The magnitude of the incident electric field is assumed to be 1 in all the calculations.

IV. MIE SCATTERING FIELD AND DIPOLAR APPROXIMATION

Consider the scattering of a linearly polarized plane wave by an Au nanosphere. The coordinate system is shown in Fig. 3(a). The origin of a Cartesian coordinate system is selected to be at the center of the nanosphere, with the incident wave propagating along the Z-axis. The incident electric field is polarized in the direction of X-axis. If the amplitude of the incident wave at the origin is E_0, the scattering field can be expressed in the form [28]

$$\overline{E}_s = \sum_{n=1}^{\infty} E_n \left[ia_n \overline{N_{e1n}} - b_n \overline{M_{01n}} \right]. \tag{5}$$

In (5), $E_n = i^n (2n+1)/(n^2+n)E_0$, a_n and b_n are the Mie scattering coefficients, and the spherical harmonics N_{e1n} and M_{o1n} are described in detail in Appendix B. Fig. 3(b) and Fig. 3(c) show the near-field and far-field scattering intensity distributions in XZ-plane outside a radiating Au nanosphere

with the radius 60nm, excited at the resonant wavelength of $540\,\text{nm}$ (corresponding to 2.3 eV in the unit of photon energy). Notice that the near-field distribution is elongated along the polarization direction; while in the far-field regime, the field spreads transverse to the polarization direction.

On the other hand, for a nanosphere with a size small compared to the wavelength, the scattering field can be approximated as being radiated from an infinitely small Hertzian dipole located at the center of the Au nanosphere. The equivalent polarization momentum of the Hertzian dipole is related to the incident electric field by the dipolar polarizability of the Au nanosphere, which can be rigorously calculated by (3). The radiation field from this dipole is then described by [29]

$$\overline{E}_r = \frac{1}{4\pi\varepsilon_0} \left\{ \frac{k^2}{r} \hat{r} \times \overline{p} \times \hat{r} + \left(\frac{1}{r^3} - \frac{ik}{r^2} \right) [3\hat{r}(\hat{r} \cdot \overline{p}) - \overline{p}] \right\} e^{ikr} \tag{6}$$

where p is the induced dipole moment of the Au nanosphere. Fig. 3(d) and Fig. 3(e) shows the intensity distributions of the near field and far field of this ideal dipole in the XY-plane, respectively. It can be seen that the dipole approximation agrees very well with the rigorous Mie theory in both near-field and far-field regimes for such a nanosphere, in terms of describing the scattering field.

V. INDUCED OPTICAL FORCE THROUGH RESONANT SCATTERING FIELD

The resonant scattering field from an Au nanosphere is quite nonuniform and decays rapidly with increasing radial distance. Such a nonuniform electric field can be utilized to exert a gradient force on another Rayleigh dielectric object close to the nanosphere. The induced optical force can be rigorously calculated by the generalized Lorentz–Mie Theory (GLMT) [30]. However, such calculations are mathematically intensive, and it is difficult to acquire an intuitive feeling of the physical phenomenon beyond the mathematics. Since the dipole model is a good approximation for Mie scattering when the nanosphere size is small compared to the wavelength, we can apply the closed-form expression in (6) to analyze the induced gradient force from the resonant scattering field.

In far-field regime, the first term in (6) dominates. The magnitude of the electric field in this region can be written as

$$E_f = \frac{k^2 |\alpha_{\text{dip}}| E_0 \sin\theta}{4\pi\varepsilon_0 r} \tag{7}$$

where θ is the intersection angle between the radial vector and the polarization vector defined in Fig. 3(a). The resulting radiation force on a Rayleigh particle can be calculated by the
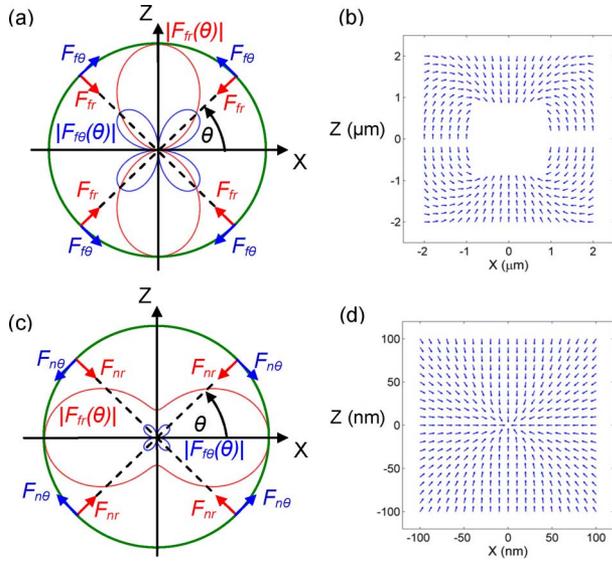
Fig. 4. (a) Direction and amplitude cross section of the radial and angular force components in the scattering far field. (b) Vector plot of the optical force induced by the scattering far field. (c) Direction and amplitude cross section of the radial and angular force components in the scattering near field. (d) Vector plot of the optical force induced by the scattering near field. The arrow length in (b) and (d) does not represent the force magnitude.

expression

$$\overline{F}_f = \frac{1}{4}\alpha_p \overline{\nabla}E_f^2 = \frac{k^4 \alpha_p |\alpha_{\text{dip}}|^2 E_0^2}{64\pi^2 \varepsilon_0^2}$$

$$\cdot \left(-\hat{r}\frac{2}{r^3}\sin^2\theta + \hat{\theta}\frac{2}{r^3}\sin\theta\cos\theta\right) \equiv F_{fr}\hat{r} + F_{f\theta}\hat{\theta} \quad (8)$$

where α_p is the polarizability of the dielectric Rayleigh particle. As shown in (8), the optical radiation force in scattering far field consists of two components: radial force F_r and angular force F_θ. The direction and amplitude cross section of the two force components are shown in Fig. 4(a). The radial force points toward the nanosphere. The direction of the angular force is determined by the sign of $\sin\theta\cos\theta$. The angular force is in the $\hat{\theta}$-direction for $0 < \theta < \pi/2$ and $\pi < \theta < 3\pi/2$, and the $-\hat{\theta}$-direction for $\pi/2 < \theta < \pi$ and $3\pi/2 < \theta < 2\pi$. The angular force points toward the $\theta = \pi/2(3\pi/2)$ equator, where its magnitude decreases to zero. The combinational effect of the radial and angular force components pulls the dielectric particle toward the angular force valley on Z-axis, shown in Fig. 4(b). If the object is elliptical in shape, its long axis will then be gradually aligned to the equator orthogonal to the polarization direction, when it approaches the radiation source.

In near-field regime, the second term in (6) dominates. The magnitude of the electric field can be expressed by

$$E_n = \frac{|\alpha_{\text{dip}}|E_0 \sqrt{(3\cos^2\theta + 1)(1/r^2 + k^2)}}{4\pi\varepsilon_0 r^2}. \quad (9)$$

The magnitude of the radiation electric field in this region is much larger here than that in the far-field regime, and decays much faster. The associated gradient force exerted on a dielectric
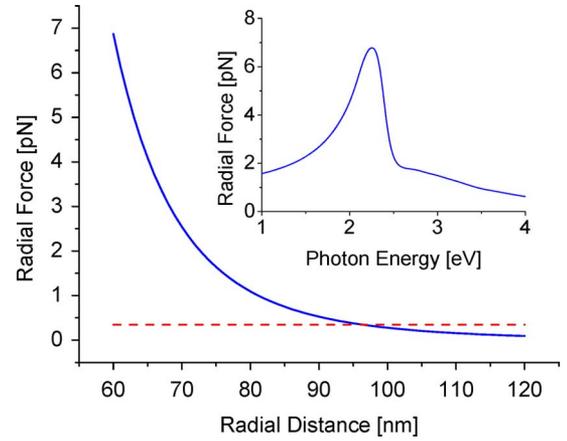

Fig. 5. Magnitude of the radial force exerted on a $60\,\text{nm}$ radius dielectric sphere with refractive index 1.59 versus the radial distance between the dielectric sphere and radiating Au nanosphere $(\theta = 0)$. The Au nanosphere is excited resonantly with an optical intensity of $0.5\,\text{mW}/\mu\text{m}^2$. The dash line represents ten times of the equivalent thermal force due to Brownian motion for the $60\,\text{nm}$ dielectric sphere. The inset shows the resonance property of this force, which has the same wavelength dependence as the dipolar polarizability of Au nanosphere.

Rayleigh particle in the near-field regime is given by

$$\overline{F}_n = \frac{1}{4}\alpha_p \overline{\nabla}E_n^2 = \frac{\alpha_p |\alpha_{\text{dip}}|^2 E_0^2}{64\pi^2 \varepsilon_0^2}\cdot\left[-\hat{r}\left(\frac{6 + 4k^2 r^2}{r^7}\right)\right.$$

$$\left.(3\cos^2\theta + 1) - \hat{\theta}\left(\frac{6 + 6k^2 r^2}{r^7}\right)\sin\theta\cos\theta\right] \equiv F_{nr}\hat{r} + F_{n\theta}\hat{\theta}.$$
$$(10)$$

We now consider the force exerted on a 60-nm radius dielectric particle with the refractive index 1.59 close to the radiating Au nanosphere. The induced optical force in radial direction is calculated by using (10) and plotted as a function of the radial distance in Fig. 5. The results show that the maximum radial force of ~ 1 pN can be achieved at a separation distance of ~ 80 nm, with an excitation light intensity of 0.5 mW/μm^2. Such intensity is several orders lower than the requirement for conventional optical tweezers to trap the same dielectric particle.

Imaging a dielectric particle that is originally located in the far-field regime of the nanosphere, it will be pulled toward the nanosphere by the induced optical force when the excitation light intensity exceeds a threshold, enters the near-field regime, and finally, arrives at the vicinity of the nanosphere. If the particle is elliptical, the long axis will be aligned to the orientation orthogonal to the polarization of the external electric field when it moves across the far-field regime, and almost keeps this orientation when it moves across the near-field regime, since the angular force is much smaller than that of the radial force in the near-field regime.

VI. SCATTERING FIELD FROM A RANDOM AU NANOSPHERE ARRAY

Although the fabrication of an isolated Au nanosphere or an ordered Au nanoparticle array can be achieved by using electron-beam lithography (EBL), the functional area is small in the former and the EBL writing time is long in the latter case.
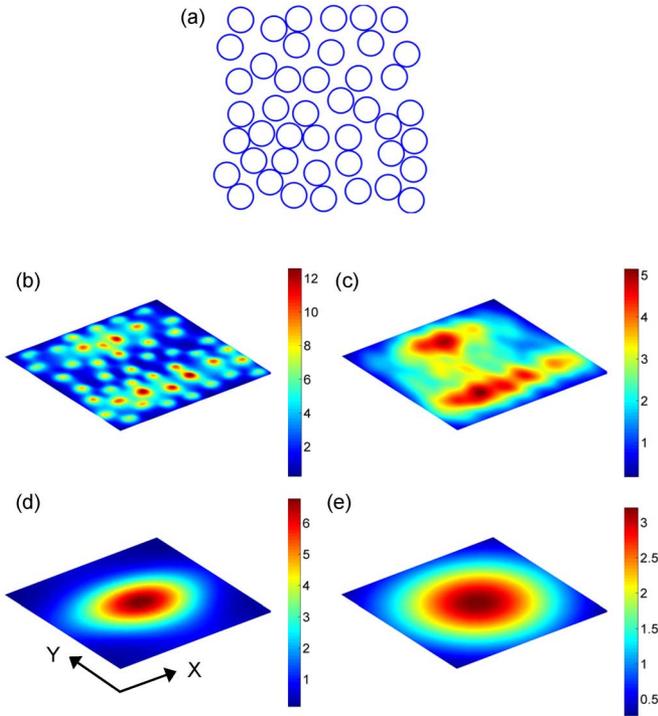
Fig. 6. (a) Au nanospheres randomly distributed on a 2D domain $1 \times 1 \, \mu m^2$. Each nanosphere ($a = 60 \, nm$). is represented by a circle. Scattering field distributions on observation planes which are parallel to the random nanosphere array are shown in (b)–(e). The nanosphere array is uniformly illuminated by a plane wave at the wavelength of 540 nm. The refractive index of the surrounding medium is 1.33. The polarization direction of the plane wave points along the X-axis. The magnitude of the incident electric field is assumed to be 1 in the calculation. The separation between the observation plane and the nanosphere array is defined as h. (b) $h = a$. c) $h = 2a$. d) $h = \lambda$. e) $h = 2\lambda$.

Therefore, we used self-assembled Au nanoparticle arrays for the described technology. We have previously reported using such approach for enhanced optical trapping of microsized particles [24], [31]. Here, we further study the scattering field from a randomly distributed Au nanosphere array.

A 2-D random Au nanosphere array is generated numerically by using the simple sequential inhibition (SSI) model [32]. Spheres with the $60 \, nm$ radius are placed sequentially at random positions in a given 2-D domain. If a new sphere is placed in such a way that it intersects any previous one, the new sphere is rejected, and a next attempt is made to place it. The process stops when the jamming coverage of the assembly reaches the designated value. This method produces random assembly of spheres that do not overlap with each other.

By treating the nanosphere unit as a dipole, the total scattering field can be determined by summing up the scattering field radiating from each individual dipole, represented by (6). Considering the random nanosphere array in Fig. 6(a) illuminated with a plane wave at the wavelength of 540 nm, we calculate the 2-D distribution of the overall field on the planes parallel to the nanosphere array at different vertical heights. When the observation plane is at the vicinity of the nanosphere array [Fig. 6(b)], the field is highly localized and a few hot spots can be observed at locations where the nanospheres are densely packed. The

field starts to become delocalized in the polarization direction when the observation plane is moved away from the nanosphere array [Fig. 6(c)]. The scattering field is further concentrated to the center of the studied domain when the observation plane is moved to the far-field regime [Fig. 6(d) and Fig. 6(e)].

Therefore, if a nanosized particle is located right above the nanosphere array, we can imagine that it will be directed by the optical force toward one of the hot spots in Fig. 6(b). This can possibly explain the surface-enhanced Raman scattering on substrates with noble metal nanostructures [33].

However, for a microsized particle, it will not be influenced by such localized fields shown in Fig. 6(b) and Fig. 6(c), since the center–center distance between the Au nanoparticle and the microsized particle is in the far-field regime. The field that the micro-sized particle feels is the scattering far field as shown in Fig. 6(e). Therefore, the microsized particle will be trapped at the center of the nanosphere array where the field maximum locates. One advantage of a nanosphere array over a single nanosphere is that the array provides much higher overall field intensity in the far-field regime, which can be used for enhanced trapping of microsized particles, such as biological cells.

VII. PLASMONIC TRAPPING EXPERIMENT

To demonstrate the optical trapping capability of single biological particles by the plasmonic scattering field, we utilize the yeast cells for preliminary experiment study. An epi-illumination microscope (Zeiss AXIO Imager DI) is used as the platform for the demonstration experiment. The Au nanoparticle array is covered by a thin liquid layer of yeast cell suspension. The fabrication process of the nanoparticle array has been discussed elsewhere [34]. A HeNe laser is directed into the optical path of the microscope and focused onto the surface of nanoparticle array by a $20\times$ objective with a low numerical aperture (NA = 0.22). The diameter of the focused light spot is measured to be $6.7 \, \mu m$. The induced LSP decays radiatively and forms the scattering field, which enables the stable trapping of a single microsized yeast cell, as discussed in Section VI. Fig. 7(a) shows such trapping behavior, where the location of the trapped cell (marked with a square) remains fixed and other yeast cells (marked with circles) move along with a motorized microscope stage. The lowest optical intensity to induce stable trapping for single yeast cells is found to be about $78.8 \, \mu W/\mu m^2$.

To quantitatively characterize the size dependence of the trapping capability of this plasmonics approach, we use the polystyrene beads with different sizes for the experiment. We measure the minimum flow rates of surrounding liquid at which the trapped particle is released from the trap as follows. The location of the trapped particle remains fixed, while the flow rate of the surrounding liquid incrementally increases (by using an external controller for the microscope stage) until the particle is released. The flow rate at which the trapped particle is released represents the threshold of the viscous drag force overcoming the trapping force, and can therefore, be used to determine the trapping force. In Fig. 7(b), this critical flow rate is plotted as a function of optical intensity for polystyrene beads with different sizes. For a 2.45-μm-diameter polystyrene bead, which
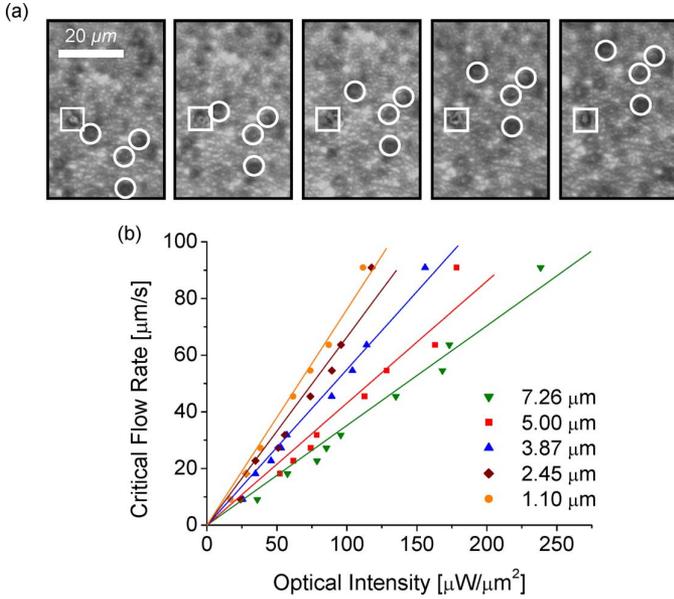
(a)

(b)

Fig. 7. (a) Single yeast cell is trapped at the location where the square marks. Other yeast cells in liquid layer are moving at a constant speed along with the piezoelectric stage of the microscope. The time period between adjacent snapshots is about 1 sec. The blur background is the random distributed Au nanoparticle array. (b) Critical flow rate to release the trapped polystyrene particle as a function of incident optical intensity.

has the size similar to the yeast cell, the lowest optical intensity to induce the stable trapping is $23.9 \, \mu W/\mu m^2$. The optical intensity required for yeast cell trapping is about three times higher than this value, which is because the cell has a refractive index closer to the liquid environment than to the polystyrene beads. The slope of the fitted line in Fig. 7(b) can be considered as an evaluation factor for the trapping stability. It can be seen that the plasmonic approach has the advantage to trap smaller particles, which is consistent with the theoretical analysis in Section V. Future trapping experiment for submicron and nanoscale particles is underway.

VIII. CONCLUSION

In summary, we have performed quantitative analysis of optical radiation force associated with the resonant scattering field from a single Au nanosphere. The modeling results indicate that single dielectric particles can be trapped and directed toward the single radiating nanosphere. This force can be utilized to develop probes for manipulation of single nanoparticles or molecules at a low-optical-intensity level. The angular component of the radiation force can align an elliptical particle with its long axis perpendicular to the polarization of the input light. Since the polarization of the input light can be tuned precisely by a polarization rotator, this force may provide the capability to control the orientation of nonspherical particles. This orientation control mechanism is based on the spatial distribution of the LSP-associated scattering field, and therefore, does not require tight focusing of incident light beam. This is fundamentally different from prior approaches utilizing azimuthally asymmetric beams [35] or birefringent properties of particles [36]–[38].

We expect to realize fine orientation control by changing light polarization through the plasmonic platform at a lower optical intensity.

The modeling results on random distributed nanosphere array show that a nanosized particle will be trapped to one of the hot spots at the vicinity of the nanosphere array. Besides strong enhancement in near field, the enhanced field intensity in far-field regime of the random distributed nanosphere array can be used for enhanced trapping of microsized particles. We have realized the trapping of single yeast cells and polystyrene beads with various sizes down to $1 \, \mu m$ by using the proposed approach. Furthermore, the proposed plasmonic platform can be integrated with the holographic optical trapping technique [39], and thus, yields parallel manipulation of very large quantities of particles at low optical powers.

APPENDIX A

The scattered power from the Au nanosphere measured at an outer spherical surface with radius r is expressed by

$$P_{\text{scat}} = \int_0^{2\pi} \int_0^{\pi} \frac{c\varepsilon_0}{2} E_{\text{rad}}^2(r, \theta) r^2 \sin\theta \, d\theta \, d\zeta \qquad (11)$$

where θ is the angle defined in Fig. 3(a), ζ is the intersection angle between Y-axis and the projection of $\hat{r}$ on YZ-plane [not shown in Fig. 3(a)], I_{scat} is the intensity of the scattering field, and c is the speed of light.

Assuming that $r \gg \lambda$ and the scattering field is contributed only by the dipolar radiation, E_{rad} in (11) can be substituted by (7), and P_{scat} in (11) becomes

$$P_{\text{scat}} = \int_0^{2\pi} \int_0^{\pi} \frac{c\varepsilon_0}{2} \left(\frac{k^2 |\alpha_{\text{dip}}| E_0 \sin\theta}{4\pi\varepsilon_0 r} \right)^2 r^2 \sin\theta \, d\theta \, d\zeta$$

$$= \frac{c |\alpha_{\text{dip}}|^2 E_0^2 k^4}{12\pi\varepsilon_0}. \qquad (12)$$

This scattered power can also be expressed by the far-field scattering efficiency

$$P_{\text{scat}} = I_{\text{inc}} Q_{\text{fsat}} \pi a^2 = \frac{c\varepsilon_0}{2} Q_{\text{fscat}} \pi a^2 E_0^2 \qquad (13)$$

where I_{inc} is the incident optical intensity. From (12) and (13), the magnitude of the dipolar polarizability of the nanosphere can be obtained by

$$|\alpha_{\text{dip}}| = \frac{\sqrt{6Q_{\text{fscat}}} \pi a \varepsilon_0}{k^2}. \qquad (14)$$

APPENDIX B

The vector spherical harmonics in (5) are expressed by

$$\overline{N}_{\text{ein}} = \frac{\cos\gamma n(n+1)\sin\delta\pi_n(\cos\delta)h_n^{(1)}(kr)}{(kr)_r}$$

$$+ \frac{\cos\gamma \tau_n(\cos\delta)[krh_n^{(1)}(kr)]'}{(kr)_\delta}$$

$$- \frac{\sin\gamma \pi_n(\cos\delta)[krh_n^{(1)}(r)]'}{(kr)\,\varphi} \qquad (15)$$

$$\overline{M}_{01n} = \cos\gamma\pi_n(\cos\delta)h_n^{(1)}(kr)\hat{\delta}$$
$$- \sin\gamma\tau_n(\cos\delta)h_n^{(1)}(kr)\hat{\varphi} \qquad (16)$$

where $h_n^{(1)}$ is the Hankel function of the first kind, $\pi_n = P_n^1/\sin\delta$ and π_n with P_n^1, being the associated Legendre functions of the first kind of degree n and order 1, and δ and γ are the angles defined in Fig. 3(a). Special care needs to be taken along the propagation direction ($\delta = 0, \pi$) because the denominators of π_n and τ_n's expression become zero. The values of π_n and τ_n in this particular direction need to be determined by expanding the associated Legendre polynomials and are given by

$$\pi_n(\delta = 0) = \frac{-1 - (n+2)(n-1)}{2}$$

$$\pi_n(\delta = \pi) = (-1)^n \left[\frac{-1 - (n+2)(n-1)}{2} \right]$$

$$\tau_n(\delta = 0) = -1 - (n+2)(n-1)/2$$

$$\tau_n(\delta = \pi) = (-1)^{n-1} \left[\frac{-1 - (n+2)(n-1)}{2} \right] \qquad (17)$$

ACKNOWLEDGMENT

REFERENCES

[1] E. Hunter and J. H. Fendler, "Exploitation of localized surface plasmon resonance," *Adv. Mater.*, vol. 16, pp. 1685–1706, 2004.

[2] S. Maier and H. A. Atwater, "Plasmonics: Localization and guiding of electromagnetic energy in metal/dielectric structures," *J. Appl. Phys.*, vol. 98, pp. 011101-1–011101-10, 2005.

[3] A. Moores and F. Goettmann, "The plasmon band in noble metal nanoparticles: An introduction to theory and applications," *New J. Chem.*, vol. 30, pp. 1121–1132, 2006.

[4] K. A. Willets and R. P. Van Duyne, "Localized surface plasmon spectroscopy and sensing," *Annu. Rev. Phys. Chem.*, vol. 58, pp. 267–297, 2007.

[5] K. Kim, S. J. Yoon, and D. Kim, "Nanowire-based enhancement of localized surface plasmon resonance for highly sensitive detection, a theoretical study," *Opt. Exp.*, vol. 14, pp. 12419–12431, 2006.

[6] S. R. Serchen, S. L. Westcott, J. L. West, and N. J. Halas, "An optomechanical nanoshell-polymer composite," *Appl. Phys. B*, vol. 73, pp. 379–381, 2004.

[7] A. R. Lowery, A. M. Gobin, E. S. Day, N. J. Halas, and J. L. West, "Immunonanoshells for targeted photothermal ablation of tumor cells," *Int. J. Nanomed.*, vol. 1, pp. 149–154, 2006.

[8] G. L. Liu, J. Kim, Y. Lu, and L. P. Lee, "Optofluidic control via photothermal nanoparticles," *Nat. Mater.*, vol. 5, pp. 27–32, 2006.

[9] X. Miao, B. Wilson, and L. Y. Lin, "Low-power induced microfluidic mixing through localized surface plasmon," in *Proc. IEEE Eng. Med. Biol. Soc. Conf.*, Lyon, France, Aug. 22–26, 2007, pp. 6306–6309.

[10] S. Maier, P. G. Kik, H. A. Atwater, S. Meltzer, E. Harel, B. E. Koel, and A. A. G. Requicha, "Local detection of electromagnetic energy transport below the diffraction limit in metal nanoparticle plasmon waveguides" *Nat. Mater.*, vol. 2, pp. 229–232, 2003.

[11] W. Srituravanich, S. Durant, H. Lee, C. Sun, and X. Zhang, "Deep subwavelength nanolithography using localized surface plasmon modes on planar silver mask," *J. Vac. Sci. Techol., B*, vol. 23, pp. 2636–2939, 2005.

[12] A. Ashkin, "Acceleration and trapping of particles by radiation pressure," *Phys. Rev. Lett.*, vol. 24, pp. 156–159, 1970.

[13] K. Svoboda and S. M. Block, "Biological applications of optical forces," *Annu. Rev. Biophys. Biomol. Struct.*, vol. 23, pp. 247–285, 1994.

[14] P. C. Chiou, A. T. Ohta, and M. C. Wu, "Massively parallel manipulation of single cells and microparticles using optical images," *Nature*, vol. 21, pp. 370–372, 2005.

[15] K. C. Neumann, E. H. Chadd, G. F. Liou, K. Bergman, and S. M. Block, "Characterization of photodamage to Escherichia coli in optical traps," *Biophys. J.*, vol. 70, pp. 1529–1533, 1996.

[16] E. J. G. Peterman, F. Gittes, and C. F. Schmidt, "Laser-induced heating in optical traps," *Biophys. J.*, vol. 84, pp. 1308–1316, 2003.

[17] G. Leitz, E. Fällman, S. Tuck, and O. Axner, "Stress response in Caenorhabditis elegans caused by optical tweezers: Wavelength, power, and time dependence," *Biophys. J.*, vol. 82, pp. 2224–2231, 2002.

[18] I. Mori and Y. Ohshima, "Molecular neurogenetics of chemotaxis and thermotaxis in the nematode," *BioEssays*, vol. 19, pp. 1055–1064, 1997.

[19] I. I. Smalyukh, D. S. Kaputa, A. V. Kachynski, A. N. Kuzmin, and P. N. Prasad, "Optical trapping of director structures and defects in liquid crystals using laser tweezers," *Opt. Exp.*, vol. 15, pp. 4359–4371, 2007.

[20] I. I. Smalyukh, A. V. Kachynski, A. N. Kuzmin, and P. N. Prasad, "Laser trapping in anisotropic fluids and polarization-controlled particle dynamics," in *Proc. Natl. Acad. Sci. USA*, vol. 103, pp. 18048–18053, 2006.

[21] L. Novotny, R. X. Bian, and X. S. Xie, "Theory of nanometric optical tweezers," *Phys. Rev. Lett.*, vol. 79, pp. 645–648, 1997.

[22] K. Okamoto and S. Kawata, "Radiation force exerted on subwavelength particles near a nanoaperture," *Phys. Rev. Lett.*, vol. 83, pp. 4534–4537, 1999.

[23] P. C. Chaumet, A. Rahmani, and M. Nieto-Vesperinas, "Optical trapping and manipulation of nano-objects with an apertureless probe," *Phys. Rev. Lett.*, vol. 88, pp. 123601-1–123601-4, 2002.

[24] X. Miao and L. Y. Lin, "Large dielectrophoresis force and torque induced by localized surface plasmon resonance of a cap-shaped Au nanoparticle array," *Opt. Lett.*, vol. 15, pp. 295–297, 2007.

[25] M. Righini, A. S. Zelenina, C. Girald, and R. Quidant, "Parallel and selective trapping in a patterned plasmonic landscape," *Nat. Phys.*, vol. 3, pp. 477–480, 2007.

[26] B. J. Messinger, K. U. Raben, R. K. Chang, and P. W. Barber, "Local fields at the surface of noble-metal microspheres," *Phys. Rev. B*, vol. 24, pp. 649–657, 1981.

[27] W. T. Doyle, "Optical properties of a suspension of metal spheres," *Phys. Rev. B*, vol. 39, pp. 9852–9858, 1989.

[28] H. Reather, *Surface Plasmons on Smooth and Rough Surfaces and on Gratings*. Berlin, Germany: Springer-Verlag, 1988.

[29] D. J. Griffiths, *Introduction to Electrodynamics*. Englewood Cliffs: Prentice-Hall, 1999.

[30] F. Ren, G. Grehan, and G. Gouesbet, "Radiation pressure forces exerted on a particle located arbitrarily in a Gaussian beam by using the generalized Lorentz-Mie theory, and associated resonance effects," *Opt. Commun.*, vol. 108, pp. 343–354, 1994.

[31] X. Miao and L. Y. Lin, "Enhanced optical trapping through localized surface plasmon resonance of Au nanoparticle array," presented at the Conf. Lasers Electro-Opt., Baltimore, MD, May 6–11, 2007.

[32] J. W. Evans, "Random and cooperative sequential adsorption," *Rev. Mod. Phys.*, vol. 65, pp. 1281–1330, 1993.

[33] F. Svedberg and M. Käll, "On the importance of optical forces in surface-enhanced Raman scattering," *Faraday Discuss.*, vol. 132, pp. 35–44, 2006.

[34] X. Miao and L. Y. Lin, "New opto-plasmonic tweezers for manipulation and rotation of biological cells—Design and fabrication," in *Proc. IEEE Eng. Med. Biol. Soc. Conf.*, New York, Aug. 30–Sep. 3, 2006, pp. 4318–4321.

[35] L. Paterson, M. P. MacDonald, J. Arlt, W. Sibbet, P. E. Bryant, and K. Dholakia, "Controlled rotation of optical trapped microscopic particles," *Science*, vol. 292, pp. 912–914, 2001.

[36] M. E. J. Friese, T. A. Nieminen, N. R. Heckenberg, and H. Rubinsztein-Dunlop, "Optical alignment and spinning of laser-trapped microscopic particles," *Nature*, vol. 394, pp. 348–350, 1998.

[37] A. I. Bishop, T. A. Tieminen, N. R. Heckenberg, and H. Rubinsztein-Dunlop, "Optical application and measurement of torque on microparticles of isotropic nonabsorbing material," *Phys. Rev. A*, vol. 68, pp. 033802-1–033802-8, 2003.

[38] A. L. Porta and M. D. Wang, "Optical torque wrench: Angular trapping, rotation, and torque detection of quartz microparticles," *Phys. Rev. Lett.*, vol. 92, pp. 190801-1–190801-4, 2004.

[39] D. G. Grier, "A revolution in optical manipulation," *Nature*, vol. 424, pp. 810–816, 2003.

Xiaoyu Miao (S'04) received the B.S. degree (with honors) in precision instruments from Tsinghua University, Beijing, China, in 2003, and the M.S. degree in electrical engineering in 2006 from the University of Washington, Seattle, where he is currently working toward the Ph.D. degree.

From 2003 to 2004, he was a Research Assistant with the Institute of Biophysics and Structural Biology, Tsinghua University, Beijing. His current research interests include biophotonics and nanophotonics.

Mr. Miao is a member of the Lasers and Electro-Optics Society (LEOS).

Lih Y. Lin (M'94–SM'02) received the Ph.D. (with highest honor) degrees in electrical engineering from the University of California, Los Angeles, in 1996.

She was a Technical Staff Member at the AT & T Laboratories-Research Senior, where she was engaged in researches on micromachined technologies for optical switching and lightwave systems. In 2000, she joined Tellium, Inc., Middlebury, IN, as the Director of optical technologies. Since 2003, she has been an Associate Professor at the Electrical Engineering Department, University of Washington, Seattle. She is the author or coauthor of more than 150 publications in refereed journals and conferences. She was the Guest Editor of the *Journal of Selected Topics in Quantum Electronics: Special Issue on Optical Micro- and Nanosystems* and the *Journal of Lightwave Technology: Special Issue on Optical MEMS and its Future Trends*. She is the holder of 22 U.S. patents.

Dr. Lin is a member of the Optical Society of America (OSA) and the American Association for the Advancement of Science (AAAS). She has served the Technical Program Committee and was the Co-Chair of various technical conferences, including the International Conference on Optical Micro-Electro-Mechanical Systems (MEMS) and Nanophotonics, the Conference on Lasers and Electro-Optics (CLEO) Pacific Rim, the IEEE Lasers and Electro-Optics Society (LEOS) Annual Meeting, the OSA Annual Meeting, and the OSA Photonics in Switching Topical Meeting. She is currently with the steering committee of the International Conference on Optical MEMS and Nanophotonics. She is the recipient of the Massachusetts Institute of Technology (MIT) Technology Review 100 Award in 2003. She was also an invitee at the National Academy of Engineering (NAE) 2005 Frontiers of Engineering Symposium.